THE JOURNAL OF PHYSICAL CHEMISTRY C

Article

Cite This: J. Phys. Chem. C 2017, 121, 22846-22853

pubs.acs.org/JPCC

Atomic-Step-Induced Local Nonequilibrium Effects on Surface Oxidation

Hailang Qin,[†] Xidong Chen,[‡] Jonathan Li,[§] Peter Sutter,[∥] and Guangwen Zhou*[,†]

[†]Department of Mechanical Engineering & Materials Science and Engineering Program, State University of New York, Binghamton, New York 13902, United States

[‡]Department of Chemistry, Physics and Engineering, Biola University, La Mirada, California 90639, United States

[§]Department of Physics, Applied Physics and Astronomy & Materials Science and Engineering Program State University of New York, Binghamton, New York 13902, United States

[∥]Department of Electrical & Computer Engineering, University of Nebraska—Lincoln, Lincoln, Nebraska 68588, United States

Supporting Information

ABSTRACT: By temperature-, time-, and pressure-resolved imaging of the dynamics of surface steps on NiAl(100) during its oxidation, we provide direct evidence of the significant effects of atomic steps in controlling the local thermodynamic driving force for oxidation. Our results show that the inherent barriers associated with step crossing by surface species of oxygen cause a heterogeneous oxygen concentration across the crystal surface, giving rise to *local* nonequilibrium effects governing oxidation even for surfaces that are *globally* in equilibrium. The asymmetry in the step-crossing barriers for oxygen atoms crossing up or down steps is such that descendant steps exert a local driving force that favors oxidation, whereas ascendant steps locally destabilize the surface oxide in their vicinity. The local differences in the thermodynamic driving force for oxidation due to atomic steps and step bunches give rise to novel phenomena, such as nonmonotonous oxide growth and the net translation motion of surface oxide stripes by growing on one end while receding on the other end.

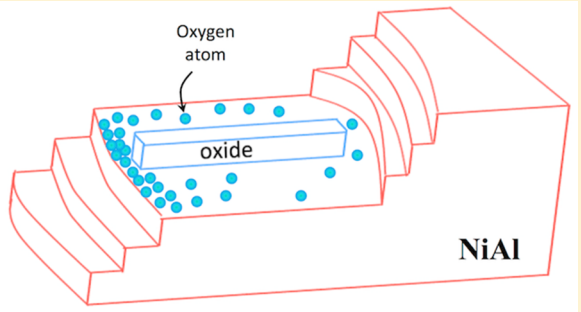

1. INTRODUCTION

Oxidation, the reaction of metals with oxygen, is an inevitable process because metals have a strong driving force to return to their low-energy oxide state. Oxidation is a rather complicated problem, and different processes, many of them coupled, are involved from the onset of reaction. Much of our current knowledge is based upon work at the mesoscale that is too coarse to reflect the underlying microscopic details of the early stages of oxidation. A detailed understanding of the key processes taking place in the critical early stages of oxidation has been hindered by overwhelming structural defects and the difficulty of probing the complex interplay between oxygen, oxide, and metal atoms at defective sites. Here we address aluminum oxide formation on a NiAl(100) surface that has a characteristic morphology common to most crystal surfaces: a series of steps alternating with flat terraces. Being able to see atomic steps and how they evolve is essential to understanding how the surface behaves in response to oxygen and elevated temperatures. Using in situ low-energy electron microscopy (LEEM) visualization of the NiAl(100) selectively oxidized in low-pressure conditions to form aluminum oxide, we show that surface steps play a significant role in promoting or suppressing oxide formation. Indeed, due to inherent barriers associated with step crossing by surface species, such as oxygen, steps can give rise to *local* nonequilibrium effects governing oxidation even for surfaces that are *globally* in equilibrium. Our results bring important new insight for atomic-scale metal oxidation in applications ranging from microelectronics and heterogeneous catalysis to protection against wear and corrosion.

NiAl is a model system for oxidation study because of its technological importance in high-temperature applications. Surface science studies have shown that the high-temperature exposure of NiAl(100) to oxygen gas results in the selective oxidation of Al atoms to form θ-like Al_2O_3 domains that form a network of elongated equally distributed oxide stripes along ⟨100⟩/⟨010⟩ directions of the NiAl(100).[1−8] Low-energy electron microscopy (LEEM) is an ideal tool to study the process of surface oxidation at near-atomic scales and to elucidate the role of different factors such as surface defects, temperature, and oxygen pressure in oxide nucleation, growth, and stability. By introducing oxygen gas to specimens under elevated temperatures, in situ LEEM imaging is capable of providing dynamic information from oxide nucleation to growth at the nanometer scale. While single-crystal surfaces

Received: July 24, 2017
Revised: September 14, 2017
Published: September 15, 2017

DOI: 10.1021/acs.jpcc.7b07321
J. Phys. Chem. C 2017, 121, 22846−22853

are usually preferred for the study of the initial stages of oxidation, the surface of a single crystal is still far from being perfect, containing a large number of defects such as atomic steps. Our understanding of the effect of these surface defects on the atomic process of oxide formation is still very limited. In situ LEEM is one of the few tools with the sufficient spatial resolution for studying the role of surface defects on the oxide nucleation and growth during the initial stages of oxidation of metals and alloys.

Using in situ LEEM, McCarty et al. studied the initial-stage oxidation of NiAl(110) and observed the formation of aluminum oxide stripes that can elongate from one substrate terrace to the next by overgrowing surface steps.[9−11] In contrast to the unimpeded oxide film growth over substrate steps on NiAl(110), we showed recently that the initial oxidation of NiAl(100) results in the unidirectional growth of aluminum oxide stripes on the same terrace that requires the coordinated migration of substrate steps.[5] This difference in the oxidation behavior in the oxidation of NiAl(100) and NiAl(110) is attributed to the different sources of Al atoms used for aluminum oxide growth; i.e., for NiAl(100), Al atoms are supplied from substrate steps via step-edge detachment,[5] while for NiAl(110), Al atoms can be supplied from the bulk via surface−bulk mass transfer.[12,13] Taking advantage of in situ LEEM for directly observing the dynamic process of the morphological evolution of oxide films during the oxidation at high temperatures, here we probe the effect of substrate steps on tuning the growth and shrinkage of Al_2O_3 stripes in response to changes in oxygen pressure and temperature. By varying oxygen pressure or temperature, we show that a "global" equilibrium can be achieved with locally non-equilibrium states induced by the effect of surface steps, for which the oxide stripes maintain their size relatively stable over time by growing at one end while decomposing at the other end.

2. EXPERIMENTAL AND COMPUTATIONAL DETAILS

A NiAl(100) single crystal (Princeton Scientific Corp.) was used for the oxidation experiments. The NiAl(100) crystal was cut to within 0.1° to the (100) crystallographic orientation and polished to a mirror finish. A clean surface can be achieved by cycles of sputtering and annealing or flashing the crystal a few times up to 1100−1200 °C. Clean ordered surfaces were verified by surface-sensitive tools including X-ray photoelectron spectroscopy (XPS),[14−16] low-energy electron diffraction (LEED), and scanning tunneling microscopy (STM) imaging.[5,6,17] Oxidation was performed by exposing the clean surface to high-purity (99.9999%) oxygen gas at temperatures ranging from 868 to 1035 °C and oxygen pressure (pO_2) in the range of 5.0×10^{-10} Torr to 2×10^{-8} Torr. The flow of oxygen gas was controlled with a variable leak valve. Real-time LEEM imaging at high temperatures during oxidation was performed in bright-field mode at an electron energy of 0.1 V. Oxygen exposure of the NiAl(100) surface at the elevated temperature results in the formation of aluminum oxide stripes. Our in situ LEEM imaging shows that the oxide stripes lengthen rapidly over time and can slowly increase their width by nucleating fine stripes alongside. This is consistent with STM imaging results, which show that the oxide stripes typically consist of multiple fine stripes of several nanometers in width and 2−4 Å in thickness.[5,6] LEED was used to confirm the formation and structure of the aluminum oxide films generated from the in situ oxidation. The LEED patterns of the oxide stripes indicated a well-ordered $(2 \times 1, 1 \times 2)$ structure,[6,17] which is in accordance with the formation of θ-Al_2O_3 films adopting the Bain epitaxy relationship between the face-centered cubic (fcc structure) of the oxygen sublattice and body-centered cubic (bcc) structure of the NiAl substrate, i.e., $(001)_{\text{O-sublattice}} \parallel (001)_{\text{NiAl}}$ and $[110]_{\text{O-sublattice}} \parallel [001]/[010]_{\text{NiAl}}$.[3,4,7,8,18−20]

Unlike the oxidation of NiAl(110) that results in strain-induced translation domain boundaries in aluminum oxide stripes,[9] no strain-induced boundaries were observed in the oxide stripes on NiAl(100) shown in this work. This difference may be due to the crystallographic orientation effect. Our previous STM study showed that the oxide stripes grow initially as isolated pairs of a double-row stripe structure, and the smallest spacing between the two rows is about 6 Å,[6] which is very close to the lattice parameter a ($a_{\theta-\text{Al2O3}}$ = 5.64 Å) of θ-Al_2O_3 along the [100] direction. It is also in agreement with the spacing of $2 \times a_{\text{NiAl}}$ (a_{NiAl} = 2.89 Å) perpendicular to the stripes in the $(2 \times 1, 1 \times 2)$ superstructure in the LEED pattern, in which the [010] direction of the θ-Al_2O_3 is parallel to the [100] direction of the NiAl. Therefore, the aluminum oxide stripes on NiAl(100) are not significantly strained because of the close lattice match between θ-Al_2O_3 and the NiAl(100) substrate (i.e., $a_{\theta-\text{Al2O3}} \cong 2\, a_{\text{NiAl}}$, and $b_{\theta-\text{Al2O3}} \cong a_{\text{NiAl}}$). Compared to the 4-fold symmetry of the NiAl(100) surface, the lower symmetry of the (110) surface may result in an interface structure that induces significant strain in the aluminum oxide stripes on NiAl(110).[9]

The density-functional theory (DFT) calculations were performed using the Vienna ab initio simulation package[21,22] with the Perdew−Burke−Ernzerhof (PBE) functional[23] and projector-augmented wave potentials[24] using a cutoff energy of 380 eV. The calculations were carried out with broadening of the Fermi surface according to Methfessel−Paxton smearing technique[25] with a smearing parameter of 0.2 eV. The oxygen atom hopping barriers of Al-terminated and Ni-terminated steps were computed for a monatomic step height on NiAl(100) using the nudged elastic band method. The structural optimization was terminated when all force components acting on the unconstrained atoms were less than 0.02 eV/Å, while the bottom two layers were fixed and the rest of the atoms free to relax. In the direction normal to the terraces, successive slabs were separated by a vacuum region of 15 Å. The Brillouin zone was sampled using a $2 \times 3 \times 1$ Monkhorst−Pack mesh.[26] Our calculated lattice constant for NiAl was 2.892 Å, which was in good agreement with ref 5 and the experimental value 2.89 Å.[27] The terraces used in the calculations included both Al-terminated and Ni-terminated and had six atomic rows along the [100] direction and four atomic rows wide in the [010] direction (more detail is given in the Supporting Information).

3. RESULTS

We probe the effect of substrate steps on the stability and size evolution of oxide stripes by varying either oxygen pressure or substrate temperature. The growth and shrinkage of aluminum oxide stripes can be observed by deliberately controlling pO_2 at elevated temperature. At a given temperature, an equilibrium pO_2 exists under which the oxide stripes remain stable in size; i.e., they neither grow nor shrink. The oxide stripes decompose if the oxygen pressure is below the equilibrium pO_2, while they grow above the equilibrium pO_2. The oxide island size remains relatively constant over time if the NiAl substrate, aluminum oxide, and gas-phase oxygen (via the adsorbed oxygen on the

DOI: 10.1021/acs.jpcc.7b07321
J. Phys. Chem. C 2017, 121, 22846−22853

substrate) are in thermodynamic equilibrium. We monitored the oxide growth and decomposition in response to changes in pO_2 by in situ LEEM imaging at several temperatures.

Figures 1(a–c) exemplify an observation (see Supporting LEEM video S1) of the growth and decomposition of Al_2O_3

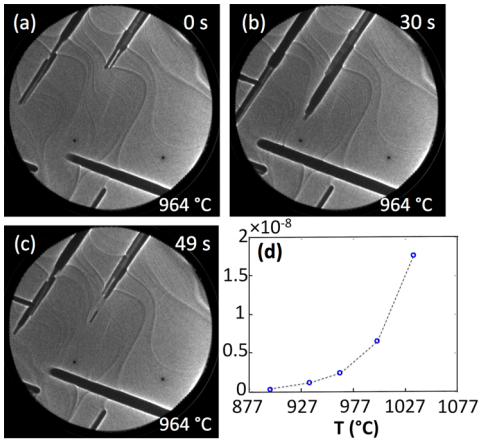

Figure 1. (a–c) Time-elapsed LEEM images (supporting in situ LEEM video S1, FOV: 10 μm) showing the growth/decomposition of Al_2O_3 stripes at T = 964 °C in response to pO_2. (a) $pO_2 = 4.7 \times 10^{-9}$ Torr. (b) $pO_2 = 4.7 \times 10^{-9}$ Torr. (c) $pO_2 = 2.4 \times 10^{-9}$ Torr. (d) pO_2 for equilibria between Al_2O_3 stripes and NiAl(100) determined by measuring pO_2 at which Al_2O_3 stripes remain stable.

stripes on NiAl(100) at 964 °C by varying pO_2. The Al_2O_3 stripes grow when $pO_2 = 4.7 \times 10^{-9}$ Torr (Figure 1(a, b)). Slightly lowering pO_2 to 2.4×10^{-9} Torr results in oxide decomposition and shrinking (Figure 1(c)). In this way, we measured the equilibrium pO_2 at several temperatures. Figure 1(d) illustrates the Al_2O_3/NiAl(100) phase equilibria determined from our in situ LEEM measurements. The equilibrium pO_2 required to stabilize the aluminum oxide stripes shown here is many orders of magnitude higher than that for α-Al_2O_3. For example, the pO_2 for maintaining equilibrium with the aluminum oxide stripes and the NiAl substrate at T = 1000 °C is ~6.5×10^{-9} Torr, while the pO_2 in equilibrium with NiAl and α- Al_2O_3 at the same temperature is 9.0×10^{-28} Torr.[10] The aluminum oxide formed under the range of temperature and pressure of our experiments has the form of θ-Al_2O_3,[5,6,17] which is a metastable polymorph of Al_2O_3. While the difference between the heat of formation of α-Al_2O_3 and θ-Al_2O_3 at bulk was shown to be marginal,[28] the ultrathin oxide film dealt in our case has the thickness less than a few Å,[5,6,17] for which the surface and interface effects such as oxide surface termination and lattice mismatch at the oxide/substrate interface play a significant role in determining the ultrathin oxide film formation. The facile decomposition of the aluminum oxide stripes can be related to the surface and interface effects that lead to the lower stability of the surface oxide.

In the previous study of the stability state of aluminum oxide on the NiAl(110) surface,[10] the energy of oxide formation was evaluated based on the thermodynamics of the oxide at bulk through a linear fit of $\ln(P)$ against $1/T$, i.e., $\ln(pO_2) = \frac{\Delta H^0}{RT} - \frac{\Delta S^0}{R}$, by omission of the surface and interface effects. It is worth mentioning that such an analysis is not applicable to the early stages of surface oxidation, where the surface and interface energies play an important role in determining the stability of the oxide film. For instance, the thickness of the aluminum oxide films dealt in our study ranges just from 2 to 4 Å,[5,6,17] for which the surface/interface area-to-volume ratio is very high. The important role of surface and interface effect in determining the thermodynamic stability is comprehensively expounded in refs 29–31 and demonstrated by experimentally observed shape transitions induced by the surface and interface effects in nanoscale systems.[32–35]

The experiments shown above demonstrate that the three-phase equilibria between adsorbed O, Al_2O_3, and the NiAl(100) substrate can be established by adjusting pO_2 at a given T. As illustrated below, local nonequilibrium states induced by microscopic features of the NiAl substrate exist within the global equilibria established by the macroscopic variables of pO_2 and T. Figures 2(a–e) show in situ LEEM images

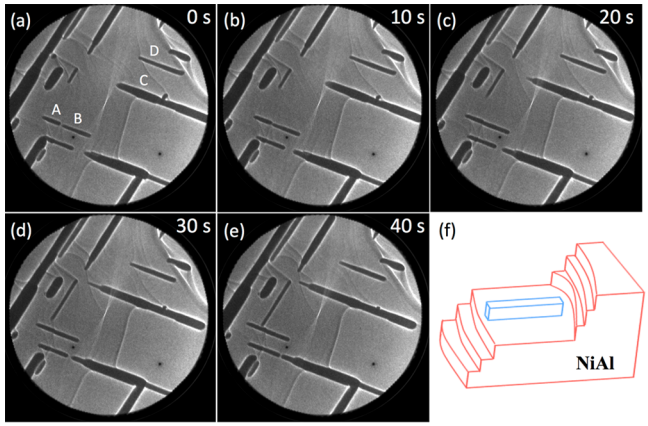

Figure 2. (a–e) Sequence of LEEM images (supporting in situ LEEM video S2, FOV: 15 μm) showing the drifting motion of oxide stripes at $pO_2 = 1.8 \times 10^{-8}$ Torr and T = 1035 °C. Substrate steps bound the two ends of the oxide stripes. (f) Pictorial illustration of the net translational motion of an oxide stripe, where the oxide stripe end facing the ascendant step decomposes while the other end facing the descendant step grows.

extracted from supporting LEEM video S2. Initially, most of the oxide stripes are growing at $pO_2 = 1.9 \times 10^{-8}$ Torr and T = 1035 °C. A slight lowering of pO_2 to 1.6×10^{-8} Torr switches the oxide stripes from growth to decomposition. This suggests that an equilibrium pO_2 exists between the two oxygen pressures identified above. Indeed, slightly increasing pO_2 to 1.8×10^{-8} Torr causes the oxide stripes to remain stable in size. Strikingly, however, the in situ LEEM observations show a peculiar way of maintaining the stable size, via growth of a new oxide at one end of the stripe while decomposing the oxide at the other end; hence the oxide stripes appear to undergo a translational motion across the surface, as seen in Figures 2(a–e) and supporting LEEM video S2. As a result, the oxide stripes still maintain their size relatively unchanged over time. This demonstrates the existence of a state that is locally out of equilibrium within the nearly overall equilibrium condition; i.e., one end of the oxide stripe is experiencing a reducing reaction that results in the oxide decomposition, while the other end of the oxide stripes is experiencing an oxidizing reaction that leads to the formation of a new oxide at the leading edge. In this way, an overall equilibrium state, for which no net growth or decomposition occurs, is maintained.

Further details of the oxide growth and decomposition under local nonequilibrium conditions can be obtained by monitoring the evolution of the two ends of oxide stripes such as A, B, C,

DOI: 10.1021/acs.jpcc.7b07321
J. Phys. Chem. C 2017, 121, 22846–22853

and D, as indicated in Figure 2(a). Both ends of the oxide stripes appear to move toward the left; i.e., the left end of the oxide stripes is growing, while the right end is decomposing. The dark curved lines in the LEEM images correspond to atomic steps of the substrate, imaged with Fresnel interference contrast.[36] Close inspection of supporting LEEM video S2 shows that the two ends of each oxide stripe are near substrate steps, and the net translation of the oxide stripes involves the coordinated migration of the bounding steps. Because the advancement and retraction at the two ends of the oxide stripes occur exclusively on the same terrace,[5] one end of the oxide stripes must face descendant steps of the substrate, while the other end of the oxide stripes faces ascendant steps of the substrate. Therefore, the oxide's growth at one end and decomposition at the other end are induced by the geometrical nature (e.g., descendant vs ascendant) of the substrate steps. In the current field of view (FOV), the substrate steps are descendant from right to left, as identified from our previous work.[5] Therefore, the left end (marked *A*) of the stripes encounters descendant steps, while the other end of the oxide stripes faces ascendant steps. As shown schematically in Figure 2(f), the oxide film is growing in the vicinity of descendant steps while decomposing in the vicinity of ascendant steps under the global thermodynamic equilibrium condition.

The in situ LEEM observations shown in Figure 2 demonstrate that the oxide stripes maintain their size relatively unchanged over time under a nearly global equilibrium in which the oxide coverage stays roughly constant. However, the presence of step bunching induces local nonequilibrium states at the two ends of the oxide stripes within the overall equilibrium condition, for which the end of the oxide stripe facing descending steps experiences the reducing reaction that results in the oxide decomposition, while the other end of the same oxide stripe in adjacent to the ascendant steps undergoes the oxidizing reaction that leads to new oxide formation at the leading edge. The atomic-step-induced departure from the thermodynamic equilibrium is further confirmed by oscillatory oxide growth in response to bunching and debunching of substrate steps, shown in Figure 3(a–c) (and supporting LEEM video S3), where the oxygen pressure is set constantly above the equilibrium pO_2 as determined and shown in Figure 1. The growth front of the oxide stripe is initially away from the step edges. With continued oxygen exposure, the growth front of the oxide stripe pushes each substrate step that it encounters to advance jointly with the step edge in its path, resulting in the bunching of an increasing number of steps in front of the oxide stripe. As more steps are piled up at the leading edge, the advancement of the oxide stripe slows down dramatically and then stops. Instead of staying completely stationary, though, the front of the oxide stripe is strikingly seen to retract from the step-bunched edge, despite the oxygen pressure that is still above the equilibrium pO_2. After retracting by ~100 nm from the step-bunched edge, the oxide stripe resumes its growth, which results in encountering the bunched steps again. The oxide stripe pushes the bunched steps to advance slightly and then undergoes another cycle of retraction/regrowth. Meanwhile, the substrate steps undergo significant bunching and debunching. Such oscillatory propagation of the leading edge of the oxide stripe in response to dynamic bunching and debunching of substrate steps is often observed in different surface regions.

Figure 3(d) shows the length evolution of the oxide stripe measured from in situ LEEM video S3. Insets in Figure 3(d)

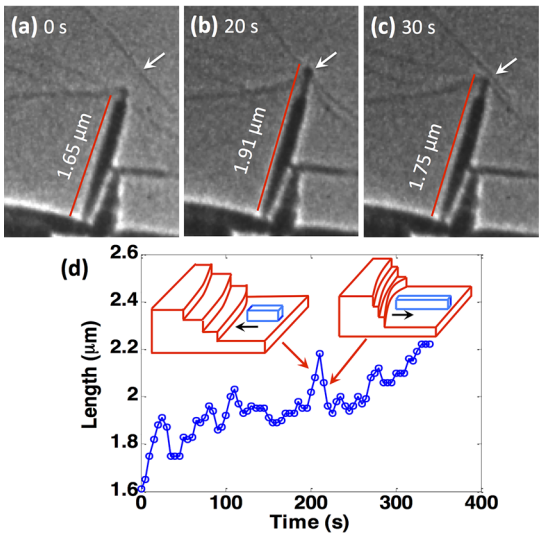

Figure 3. (a–c) Series of LEEM images (supporting in situ LEEM video 3, image size: 1.42 × 2.42 μm^2) showing that the length of an oxide stripe oscillates in a step-bunched region during oxidation at $pO_2 = 5 \times 10^{-10}$ Torr and $T = 868$ °C. The red lines mark the oxide stripe, and the arrows point to the substrate step that undergoes cyclic bunching and debunching as the oxide stripe as the oxide undergoes oscillatory lengthening. (d) Evolution of the length of the oxide stripe extracted from *in situ* LEEM movies showing the oscillatory behavior. Insets show schematically the two key stages of the observed oscillation.

show schematically the key stages of the observed oscillation: (I) The advancement of the growth front of the oxide stripe results in the encounter of several steps in its path, and (II) the progressive pileup of substrate steps in front of the leading edge switches the front of the oxide stripe from an oxidizing to a reducing condition, which results in decomposition of the oxide at the front and thus the retraction of the leading edge of the oxide stripe from the bunched steps. The retraction from the bunched steps by some distance (accompanied by the debunching of the piled steps) restores the oxidizing condition at the oxide growth front. The oxide stripe therefore resumes its growth and catches up with the steps again. Therefore, the oxide stripe oscillates in its length, i.e., undergoing growth and decomposition cycles modulated by the bunching/debunching of the substrate steps in front of the leading edge of the oxide stripe. Because the NiAl(100) surface is under the oxygen pressure that is above the equilibrium pO_2, the length of the oxide stripe shows a net increase over a longer time period (Figure 3(a,b)). It should be noted that the observed oscillation in the oxide length in Figure 3 is not related to any thermodynamic fluctuations or a kinetically random process, under which the oxide decomposition should occur at any places of the surface. Instead, our in situ LEEM observation (supporting LEEM video S3) shows that the oscillatory oxide growth occurs only in the step-bunched region, and by contrast, the oxide stripes bounded with fewer steps do not show length oscillation in the same FOV. Additionally, the observed translation motion of oxide stripes by oxide formation at one end of the oxide stripe and oxide decomposition at the other end involves the coordinated migration of substrate steps that bound with the two ends of the oxide stripes (Figure 2). Such a well-coordinated behavior at the two ends of the same oxide stripe bears no resemblance with thermodynamic fluctuations or a kinetically random process.

DOI: 10.1021/acs.jpcc.7b07321
J. Phys. Chem. C 2017, 121, 22846–22853

Our in situ LEEM observations above show that the oxide growth and decomposition involve massive migration of substrate steps. This is because the NiAl substrate steps are the source of Al atoms for aluminum oxide growth and sinks of Al atoms for aluminum oxide decomposition. Unbunched NiAl substrate steps have been shown to have the step height of ∼3 Å,[5] which is close to the lattice constant (2.89 Å) of NiAl. The surface movement of the unit-cell-height steps by the step-edge detachment and attachment involves the alternate formation of Al-terminated and Ni-terminated step edges. The supply of Al atoms from the step edges for aluminum oxide growth results in the forward movement of substrate steps and thus step bunching with the simultaneous dissolution of Ni atoms in the NiAl bulk, as evidenced by the absence of Ni clustering during the oxide growth (and also in accordance with a previous study showing the oxidation-induced dissolution of Ni in the NiAl bulk.[37−40] This process is reversed during the oxide decomposition, where Al atoms released from the decomposing oxide diffuse and reattach to the step edges of the NiAl substrate, thereby resulting in debunching of the piled steps in front of the oxide stripes. In this step-debunching process, Ni atoms attaching to the step edges are supplied from the NiAl bulk because of the large tendency of Al and Ni atoms to form strong partially covalently bonded intermetallic compounds in the Ni−Al system.[41,42] Therefore, only half of the atoms involved in the mobility of substrate steps participate in the oxide growth or decomposition, and the other half (i.e., Ni atoms) either dissolve in the bulk during oxide growth induced bunching of substrate steps or migrate from the bulk and join the step edges in the course of the oxide decomposition induced debunching of substrate steps. For this reason, significant mass exchange is involved for both the oxide growth and decomposition. Because substrate steps serve both as the sources of Al atoms for aluminum oxide growth and as the sinks of Al atoms during the aluminum oxide decomposition, the advancement (oxide growth) and retraction (oxide decomposition) of the leading edge of the oxide stripes drive the coordinated reconfiguration of the substrate steps, as seen from Figures 1−3 and supporting in situ LEEM videos.

4. DISCUSSION

Our in situ LEEM observations show that the oxide growth and decomposition occur only at the leading edge of the oxide stripes. In view of the massive surface mobility of substrate steps arising from the highly efficient mass transfer from and to atomic steps at the high temperature, we make an assumption that the oxide growth and decomposition are governed by the surface diffusion of adsorbed oxygen atoms to the leading edge of the oxide stripes because of the low oxygen gas pressure in our experiment. When the surface is exposed to O_2, oxygen molecules arriving from the gas phase dissociatively adsorb to give rise to an average concentration, C, of oxygen atoms on the metal surface. Depending on the value of C relative to the equilibrium oxygen atom concentration, C_e, the aluminum oxide either grows ($C > C_e$) or decomposes ($C < C_e$). The chemical potential of oxygen atoms, μ_O, the free energy difference between an isolated oxygen atom and an oxygen atom in the oxide, is given by $\mu_O = k_B T \ln\left(\frac{C}{C_e}\right)$.[43] It is worthwhile mentioning that the oxygen chemical potential given by the gas phase is a less relevant quantity because of the low oxygen pressure employed in the present study, for which the oxide growth occurs via surface diffusion of oxygen atoms adsorbed on the substrate to the growth front of the oxide stripe instead of direct impingement of gaseous oxygen onto the oxide. When the surface is exposed to a higher pO_2, the surface density of oxygen atoms becomes supersaturated to a concentration $C > C_e$, and thus $\mu_O > 0$. The surface is therefore under an overall oxidizing condition, and the oxide stripes grow by incorporating oxygen atoms from the surrounding areas to their leading edge. Lowering pO_2 can cause $C < C_e$, and thus $\mu_O < 0$. The surface therefore changes to an overall reducing condition, and the oxide stripes then undergo decomposition at their leading edge. By carefully adjusting pO_2, we can reach $C = C_e$, and thus $\mu_O = 0$, under which the oxide stripe maintains a stable size (Figure 2).

However, the presence of surface steps complicates the oxide growth because of additional kinetic barriers (e.g., Ehrlich−Schwoebel (ES) barrier)[44,45] that hinder the crossing of oxygen atoms via a step to a lower terrace. There are two most important kinetic energy parameters involved in surface growth process, i.e., the surface diffusion barrier and the ES step edge barrier. The former controls the mass transport on terraces, and the latter controls the mass transport between terraces. The ES barrier represents the extra energy barrier for an adatom crossing over a step edge, i.e., transport from one terrace to another; its existence is ubiquitous for a wide range of surface phenomena ranging from thin-film growth[46,47] to self-assembly of nanostructures[48−50] and gas−surface reactions.[51,52] The correlation between the oxide growth and decomposition and the geometrical nature (ascendant vs descendent) of the substrate steps shown from our in situ LEEM observations clearly points to the effect of the substrate steps in modulating the surface concentration of oxygen atoms and thus the thermodynamic driving force of the surface oxidation. This is confirmed by our DFT and analytic modeling of such a surface step effect (i.e., the ES barrier), as shown below, in controlling the surface transport of oxygen atoms and surface concentration of oxygen atoms across bunched steps.

We performed DFT calculations to evaluate the magnitude of the ES barrier in our system, and found that the step-edge crossing barriers for a monatomic step are −0.40 and 0.15 eV, respectively, for ascendant and descendant step crossing. We also found that the oxygen descendant step crossing barrier was 0.69 eV greater than that of the ascendant step crossing for a multilayer step edge (more detail in the Supporting Information). In the vicinity of bunched steps, the oxygen concentration can be analytically derived as

$$c = \frac{c_0}{N+1}\sum_{n=0}^{N}\gamma^n \tag{1}$$

where C_0 is the oxygen concentration for a flat terrace far away from any step; N is the number of bunched steps; and $N = L/W - 1$ (L is the lateral width of the step-bunched region, and W is the width of a single terrace within the stepped region, as shown in Figure 4(a)) (more detail in the Supporting Information). γ is directly related to the ES barrier and given by

$$\gamma = 1 + \frac{a}{W}\left[\exp\left(-\frac{E_{ES}}{k_B T}\right) - 1\right] \tag{2}$$

where a is the lattice constant and E_{ES} is the ES barrier. By inserting the ES barriers into eq 2, we obtain the oxygen concentration and its dependence on the number of bunched steps. Figure 4(b) gives the results of the calculations using eqs

DOI: 10.1021/acs.jpcc.7b07321
J. Phys. Chem. C 2017, 121, 22846−22853

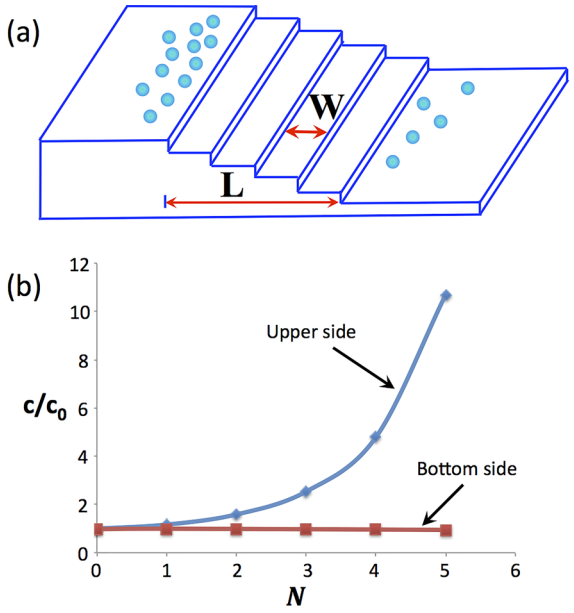

Figure 4. (a) Schematic showing the step bunching and the resulting asymmetric concentration of O atoms across bunched steps. *L*: width of the step-bunched region, *W*: width of a single terrace within the stepped region. (b) Ratio of the concentrations (C) of O atoms on the upper and lower terraces adjacent to a bunch of N steps to the concentration (C_0) on a flat terrace far from surface steps. The step bunching results in asymmetric concentrations of O atoms across bunched steps with accumulation of O atoms on the upper terrace adjacent to the step bunch.

1 and 2, which show c/c_0, the ratio of the concentration of oxygen atoms on the upper or lower ends of the step bunch with respect to the oxygen concentration on a flat terrace (N = 0). The oxide growth-induced step bunching results in an asymmetrical oxygen concentration across the bunched steps, with oxygen concentration maximal on the upper side of the bunched steps, whereas the oxygen concentration at the bottom is low, as illustrated schematically in Figure 4(a) and confirmed by the results of our analytical modeling in Figure 4(b). After multiple ascendant steps are piled up in front of an oxide stripe, the low oxygen concentration causes the oxide growth to slow down and then completely stop. The local concentration can become sufficiently low that the oxide begins to decompose, leading to the receding of the leading edge of the oxide stripe from the bunched steps. This transition from oxide growth to decomposition is induced by the step bunching that results in gradual decrease of the concentration of oxygen atoms on the lower side of the bunched steps, which switches the oxygen chemical potential from $\mu_O > 0$ to $\mu_O = 0$ and then to $\mu_O < 0$ in the immediate vicinity of the step bunch. The oxide decomposition stops after the leading edge of the oxide stripe is retracted to the location where the concentration of adsorbed O atoms is again equal to C_e. Meanwhile, Al atoms released from the decomposing aluminum oxide diffuse and reattach to the nearest substrate step edge, which results in the debunching of the steps with the reattachment of Ni atoms from the NiAl bulk (Figures 3(a–c)). This step-debunching process decreases the number of steps in the bunch and promotes the step crossing of oxygen atoms to the lower terrace where the oxide stripe resides. As a result, the concentration of oxygen atoms on the lower side of the steps increases again to $C > C_e$, allowing the oxide stripe to resume its growth. With the advancement of the oxide stripe, it encounters the substrate steps again, thereby initiating another decomposition/growth cycle.

Individual aluminum oxide stripes exist exclusively on the same atomic terrace.[5] This causes an asymmetric situation in which one front of the stripe faces ascendant steps, while the other end must face descendant steps (Figure 3). Because of the ES barrier's effect in hindering atomic transfer from the upper to the lower terrace, the surface near the front adjacent to the ascendant steps has lower oxygen concentration than the area next to the descendant steps. While adjusting pO_2 can allow the surface to reach a *global* equilibrium condition for the extended terrace regions away from atomic steps, *local* nonequilibrium conditions and a gradient in the oxygen concentration exist in the vicinity of bunched steps. Since oxide stripes cannot cross steps, their expansion invariably causes the formation of step bunches, which in turn creates a heterogeneous oxygen concentration. The consequences of this local nonequilibrium situation include, for instance, the oxidation/reduction cycles of the leading edge of the oxide stripes discussed above and the net translational motion of oxide stripes when the stripe end facing ascendant steps experiences reducing conditions ($C < C_e$), while the other end facing descendant steps experiences oxidation ($C > C_e$). As a result, the oxide stripe undergoes net motion toward the ascendant step side at constant length of the stripe, i.e., under global equilibrium conditions.

5. CONCLUSIONS

Step-crossing barriers are typically considered as a kinetic factor in controlling surface mass transport. Here we show the significant effects of atomic steps in tuning the local thermodynamic driving force for oxidation. Our results show that step-crossing barriers can cause a heterogeneous oxygen concentration across the surface, and the asymmetry in step-crossing barriers for oxygen atoms crossing up- or down-steps is such that descendant steps exert a local driving force that favors oxidation; however, ascendant steps locally destabilize the surface oxide in their vicinity. The broader applicability of the fundamental insight extracted from the present study can be expected because of the inherent barriers associated with step crossing by surface species and the match between the experimental observation and the prediction by our analytic modeling that is not tied to a specific material system.

■ ASSOCIATED CONTENT

Supporting Information

The Supporting Information is available free of charge on the ACS Publications website at DOI: 10.1021/acs.jpcc.7b07321.

SI-1. Density-functional theory calculations of Ehrlich–Schwoebel barriers **SI-2.** Solution for the surface concentration of adatoms in the vicinity of bunched steps (PDF)

SI-3: Supplemental in situ LEEM movie S1 (the movie from which Figure 1 is extracted): In situ LEEM movie (Field of View: 10 μm) showing the growth and decomposition of aluminum oxide stripes at T = 964 °C due to variations in oxygen pressure between $pO_2 = 2.4 \times 10^{-9}$ Torr and $pO_2 = 4.7 \times 10^{-9}$ Torr. The movie is accelerated by a factor of 5 of the real time (MOV)

SI-4: Supplemental in situ LEEM movie S2 (the movies from which Figure 2 is extracted): In situ LEEM movie (Field of View: 15 μm) showing the simultaneous local

DOI: 10.1021/acs.jpcc.7b07321
J. Phys. Chem. C 2017, 121, 22846–22853

growth and decomposition at $pO_2 = 1.8 \times 10^{-8}$ Torr and $T = 1035$ °C. The movie is accelerated by a factor of 5 of the real time (MOV)

SI-5: Supplemental in situ LEEM movie S3 (the movie from which Figure 3(a−e) is extracted): In situ LEEM movie (Field of View: 10 μm) showing the oscillatory growth of an oxide stripe during oxidation at $pO_2 = 5 \times 10^{-10}$ Torr and $T = 868$ °C. The movie is accelerated by a factor of 10 of the real time (MOV)

AUTHOR INFORMATION

Corresponding Author

*E-mail: gzhou@binghamton.edu.

ORCID

Peter Sutter: 0000-0002-3301-309X

Guangwen Zhou: 0000-0002-9243-293X

Notes

The authors declare no competing financial interest.

ACKNOWLEDGMENTS

This work was supported by the U.S. Department of Energy, Office of Basic Energy Sciences, Division of Materials Sciences and Engineering under Award No. DE-SC0001135. P.S. acknowledges the support from the U.S. Department under Award No. DE-SC0016343. This research used resources of the Center for Functional Nanomaterials, which is a U.S. DOE Office of Science Facility, at Brookhaven National Laboratory under Contract No. DE-SC0012704. This work used the computational resources from the Extreme Science and Engineering Discovery Environment (XSEDE), which is supported by National Science Foundation grant number OCI-1053575.

REFERENCES

(1) Blum, R.-P.; Ahlbehrendt, D.; Niehus, H. Growth of Al_2O_3 Stripes in NiAl(001). *Surf. Sci.* **1998**, *396*, 176−188.

(2) Blum, R.-P.; Niehus, H. Initial Growth of Al_2O_3 on NiAl(001). *Appl. Phys. A: Mater. Sci. Process.* **1998**, *66*, S529−S533.

(3) Fremy, N.; Maurice, V.; Marcus, P. X-ray Photoelectron Spectroscopy Study of Thin Oxide Layers Formed on (001)-Oriented NiAl Single-Crystal Surfaces. *Surf. Interface Anal.* **2002**, *34*, 519−523.

(4) Fremy, N.; Maurice, V.; Marcus, P. Initial Stages of Growth of Alumina on NiAl(001) at 1025 K. *J. Am. Ceram. Soc.* **2003**, *86*, 669−675.

(5) Qin, H. L.; Chen, X. D.; Li, L.; Sutter, P. W.; Zhou, G. W. Oxidation-Driven Surface Dynamics on NiAl(100). *Proc. Natl. Acad. Sci. U. S. A.* **2015**, *112*, E103−E109.

(6) Qin, H. L.; Zhou, G. W. The Formation of Double-Row Oxide Stripes During the Initial Oxidation of NiAl(100). *J. Appl. Phys.* **2013**, *114*, 083513.

(7) Stierle, A.; Formoso, V.; Comin, F.; Franchy, R. Surface X-ray Diffraction Study on the Initial Oxidation of NiAl(100). *Surf. Sci.* **2000**, *467*, 85−97.

(8) Stierle, A.; Formoso, V.; Comin, F.; Schmitz, G.; Franchy, R. Oxidation of NiAl(100) Studied with Surface Sensitive X-ray Diffraction. *Phys. B* **2000**, *283*, 208−211.

(9) McCarty, K. F.; Pierce, J. P.; Carter, C. B. Translation-Related Domain Boundaries Form to Relieve Strain in a Thin Alumina Film on NiAl(110). *Appl. Phys. Lett.* **2006**, *88*, 141902.

(10) Pierce, J. P.; Bartelt, N. C.; Stumpf, R.; McCarty, K. F. Stability of Ultrathin Alumina Layers on NiAl(110). *Phys. Rev. B: Condens. Matter Mater. Phys.* **2008**, *77*, 195438.

(11) Pierce, J. P.; McCarty, K. F. Self-Assembly and Dynamics of Oxide Nanorods on NiAl(110). *Phys. Rev. B: Condens. Matter Mater. Phys.* **2005**, *71*, 125428.

(12) McCarty, K. F.; Nobel, J. A.; Bartelt, N. C. Vacancies in Solids and the Stability of Surface Morphology. *Nature* **2001**, *412*, 622−625.

(13) McCarty, K. F.; Nobel, J. A.; Bartelt, N. C. Surface Dynamics Dominated by Bulk Defects: The Case of NiAl(110). *Phys. Rev. B: Condens. Matter Mater. Phys.* **2005**, *71*, 085421.

(14) Liu, Q. Q.; Qin, H. L.; Boscoboinik, J.; Zhou, G. W. A Comparative Study of Oxidation of NiAl(100) by Molecular Oxygen and Water Vapor Using Ambient-Pressure X-ray Photoelectron Spectroscopy. *Langmuir* **2016**, *32*, 11414−11421.

(15) Cai, N.; Liu, Q. Q.; Tong, X.; Zhou, G. W. X-ray Photoelectron Spectroscopic Study of the Passivation of NiAl(100) Surface by Water Vapor. *Langmuir* **2014**, *30*, 774−783.

(16) Cai, N.; Qin, H. L.; Xiao, T.; Zhou, G. W. Growth of Ultrathin Amorphous Alumina Films During the Oxidation of NiAl(100). *Surf. Sci.* **2013**, *618*, 20−26.

(17) Qin, H. L.; Sutter, P.; Zhou, G. W. The Crystallization of Amorphous Aluminum Oxide Thin Films Grown on NiAl(100). *J. Am. Ceram. Soc.* **2014**, *97*, 2762−2769.

(18) Gassmann, P.; Franchy, R.; Ibach, H. Investigations on Phase Transitions Within Thin Al_2O_3 Layers on NiAl(001) - HREELS on Aluminum Oxide Films. *Surf. Sci.* **1994**, *319*, 95−109.

(19) Maurice, V.; Fremy, N.; Marcus, P. Hydroxylation-Induced Modifications of the Al_2O_3/NiAl(001) Surface at Low Water Vapor Pressure. *Surf. Sci.* **2005**, *581*, 88−104.

(20) Stierle, A.; Formoso, V.; Comin, F.; Schmitz, G.; Franchy, R. Oxidation of NiAl(100) Studied with Surface Sensitive X-ray Diffraction. *Phys. B* **2000**, *283*, 208.

(21) Kresse, G.; Furthmuller, J. Efficiency of Ab-Initio Total Energy Calculations for Metals and Semiconductors Using a Plane-Wave Basis Set. *Comput. Mater. Sci.* **1996**, *6*, 15−50.

(22) Kresse, G.; Hafner, J. Ab Initio Molecular-Dynamics Simulation of the Liquid-Metal-Amorphous-Semiconductor Transition in Germanium. *Phys. Rev. B: Condens. Matter Mater. Phys.* **1994**, *49* (20), 14251−14269.

(23) Hammer, B.; Hansen, L. B.; Norskov, J. K. Improved Adsorption Energetics Within Density-Functional Theory Using Revised Perdew-Burke-Ernzerhof Functionals. *Phys. Rev. B: Condens. Matter Mater. Phys.* **1999**, *59* (11), 7413−7421.

(24) Kresse, G.; Joubert, D. From Ultrasoft Pseudopotentials to the Projector Augmented-Wave Method. *Phys. Rev. B: Condens. Matter Mater. Phys.* **1999**, *59* (3), 1758−1775.

(25) Methfessel, M.; Paxton, A. T. High-Precision Sampling for Brillouin-Zone Integration in Metals. *Phys. Rev. B: Condens. Matter Mater. Phys.* **1989**, *40* (6), 3616−3621.

(26) Monkhorst, H. J.; Pack, J. D. On Special Points for Brillouin-Zone Integrations. *Phys. Rev. B* **1976**, *13*, 5188−5192.

(27) Blum, R.-P.; Ahlbehrendt, D.; Niehus, H. Preparation-Dependent Surface Composition and Structure of NiAl(001): SPA-LEED and NICISS Study. *Surf. Sci.* **1996**, *366* (1), 107−120.

(28) Lodziana, Z.; Parlinski, K. Dynamical Stability of the α and θ Phases of Alumina. *Phys. Rev. B: Condens. Matter Mater. Phys.* **2003**, *67*, 174106.

(29) Goldenfeld, N. *Lectures on Phase Transitions and the Renormalization Group*; Addison-Wesley Publishing Company: 1992.

(30) Hill, T. L. *An Introduction to Statistical Thermodynamics*; Dover Publications: Mineola, 1987.

(31) Hill, T. L. *Thermodynamics of Small Systems*; Dover Publications: 2013.

(32) Tersoff, J.; Tromp, R. M. Shape transition in growth of strained islands: Spontaneous Formation of Quantum Wires. *Phys. Rev. Lett.* **1993**, *70*, 2782−2785.

(33) Brongersma, S. H.; Castell, M. R.; Perovic, D. D. Zinke-Allmang, Stress-Induced Shape Transition of $CoSi_2$ Clusters on Si(100). *Phys. Rev. Lett.* **1998**, *80*, 3795−3798.

DOI: 10.1021/acs.jpcc.7b07321
J. Phys. Chem. C 2017, 121, 22846−22853

(34) Zhou, G. W.; Yang, J. C. Formation of Quasi-One-Dimensional Cu_2O Structures by In Situ Oxidation of Cu(100). *Phys. Rev. Lett.* **2002**, *89*, 106101.
(35) Daruka, I.; Grossauer, C.; Springholz, G.; Tersoff, J. Equilibrium Phase Diagrams for the Elongation of Epitaxial Quantum Dots into Hut-Shaped Clusters and Quantum Wires. *Phys. Rev. B: Condens. Matter Mater. Phys.* **2014**, *89*, 235427.
(36) Altman, M. S.; Chung, W. F.; Liu, C. H. LEEM Phase Contrast. *Surf. Rev. Lett.* **1998**, *5*, 1129−1141.
(37) Finnis, M. W.; Lozovoi, A. Y.; Alavi, A. The Oxidation of NiAl: What Can We Learn From Ab Initio Calculations? *Annu. Rev. Mater. Res.* **2005**, *35*, 167−207.
(38) Freund, H.-J. Adsorption of Gases on Complex Solid Surfaces. *Angew. Chem., Int. Ed. Engl.* **1997**, *36*, 452−475.
(39) Jaeger, R. M.; Kuhlenbeck, H.; Freund, H.-J. Formation of a Well-Ordered Sluminum Oxide Overlayer by Oxidation of NiAl(110). *Surf. Sci.* **1991**, *259*, 235−252.
(40) Katter, U. J.; Schlienz, H.; Beckendorf, M.; Freund, H.-J. Electron Spin-Resonance (ESR) Studies of Adsorbate Dynamics on Dingle Crystal Durfaces: Possibilities and Limitations. *Ber. Bunsenges. Phys. Chem.* **1993**, *97*, 340−352.
(41) Wang, Y.; Liu, Z.-K.; Chen, L.-Q. Thermodynamic Properties of Al, Ni, NiAl, and Ni_3Al from First-Principles Calculations. *Acta Mater.* **2004**, *52*, 2665.
(42) Heinz, K.; Hammer, L. Surface Structure and Segregation of Bimetallic BCC-Type Alloys. *J. Phys.: Condens. Matter* **1999**, *11*, 8377.
(43) Tromp, R. M.; Hannon, J. B. Thermodynamics of Nucleation and Growth. *Surf. Rev. Lett.* **2002**, *9*, 1565−1593.
(44) Ehrlich, G.; Hudda, F. G. Atomic Vew of Surface Self-Diffusion: Tungsten on Tungsten. *J. Chem. Phys.* **1966**, *44*, 1039−1049.
(45) Schwoebel, R. L.; Shipsey, E. J. Step Motion on Crystal Surfaces. *J. Appl. Phys.* **1966**, *37*, 3682−3686.
(46) Zhang, Z.; Lagally, M. G. Atomistic Processes in the Early Stages of Thin-Film Growth. *Science* **1997**, *276*, 377−383.
(47) Zhu, W. G.; de Mongeot, F. B.; Valbusa, U.; Wang, E.; Zhang, Z. Adatom Ascending at Step Edges and Faceting on FCC Metal (110) surfaces. *Phys. Rev. Lett.* **2004**, *92* (10), 106102.
(48) Liu, S. J.; Huang, H. C.; Woo, C. H. Schwoebel-Ehrlinch Barrier- From Two to Three Dimensions. *Appl. Phys. Lett.* **2002**, *80*, 3295−3297.
(49) Zhang, R. X.; Huang, H. C. Another Kinetic Mechanism of Stabilizing Multiple-Layer Surface Steps. *Appl. Phys. Lett.* **2011**, *98*, 221903.
(50) Johansen, C. G.; Huang, H. C. Effects of Three-Dimensional Ehrlich-Schwoebel Barrier on Texture Selection during Cu Nanorod Growth. *Appl. Phys. Lett.* **2007**, *91*, 121914.
(51) Zhu, Q.; Saidi, W. A.; Yang, J. C. Step-Edge Directed Metal Oxidation. *J. Phys. Chem. Lett.* **2016**, *7*, 2530−2536.
(52) Zhu, Q.; Saidi, W. A.; Yang, J. C. Enhanced Mass Transfer in the Step Edge Induced Oxidation on Cu(100) Surface. *J. Phys. Chem. C* **2017**, *121* (21), 11251−11260.

DOI: 10.1021/acs.jpcc.7b07321
J. Phys. Chem. C 2017, 121, 22846−22853